



**QUEEN'S
UNIVERSITY
BELFAST**

Comparative assessment of visible light and UV active photocatalysts by hydroxyl radical quantification

Nagarajan, S., Skillen, N. C., Fina, F., Zhang, G., Randhorn, C., Lawton, L. A., Irvine, J. T. S., & Robertson, P. K. J. (2017). Comparative assessment of visible light and UV active photocatalysts by hydroxyl radical quantification. *Journal of Photochemistry and Photobiology A: Chemistry*, 334, 13-19.
<https://doi.org/10.1016/j.jphotochem.2016.10.034>

Published in:

Journal of Photochemistry and Photobiology A: Chemistry

Document Version:

Peer reviewed version

Queen's University Belfast - Research Portal:

[Link to publication record in Queen's University Belfast Research Portal](#)

Publisher rights

© 2016 Elsevier Ltd. This manuscript version is made available under the CC-BY-NC-ND 4.0 license <http://creativecommons.org/licenses/by-nc-nd/4.0/> which permits distribution and reproduction for non-commercial purposes, provided the author and source are cited.

General rights

Copyright for the publications made accessible via the Queen's University Belfast Research Portal is retained by the author(s) and / or other copyright owners and it is a condition of accessing these publications that users recognise and abide by the legal requirements associated with these rights.

Take down policy

The Research Portal is Queen's institutional repository that provides access to Queen's research output. Every effort has been made to ensure that content in the Research Portal does not infringe any person's rights, or applicable UK laws. If you discover content in the Research Portal that you believe breaches copyright or violates any law, please contact openaccess@qub.ac.uk.

Comparative assessment of visible light and UV active photocatalysts by hydroxyl radical quantification

Sanjay Nagarajan^{1*}, Nathan C. Skillen¹, Federica Fina², Guan Zhang², Chamnan Randorn², Linda A. Lawton³, John T.S. Irvine² and Peter K.J. Robertson^{1*}

¹ Centre for the Theory and Application of Catalysis (CentTACat), School of Chemistry and Chemical Engineering, Queen's University Belfast, David Keir Building, Stranmillis Road, Belfast, BT9 5AG, United Kingdom;

² JTSI Group, University of St. Andrews, School of Chemistry, Purdie Building, North Haugh, St Andrews, KY16 9ST, United Kingdom;

³ School of Pharmacy and Life sciences, Sir Ian Wood Building Robert Gordon University, Garthdee Road, Aberdeen, AB10 7GJ, United Kingdom

*Corresponding authors, *p.robertson@qub.ac.uk*; *snagarajan01@qub.ac.uk*, Tel: +44 (0) 28 9097 4627

ABSTRACT

A simple method for determining hydroxyl radical yields on semiconductor photocatalysts is highly desirable, especially when comparing different photocatalyst materials. This paper reports the screening of a selection of visible light active photocatalysts such as Pt-C₃N₄, 5% LaCr doped SrTiO₃, Sr_{0.95}Cr_{0.05}TiO₃ and Yellow TiO₂ and compares them against WO₃ and ultra violet (UV) light activated TiO₂ P25 (standard commercial catalysts) based on their oxidative strengths (OH radical producing capability) using a well-studied chemical probe – coumarin. 7-hydroxycoumarin, the only fluorescent hydroxylation product of this reaction can then be measured to indirectly quantify the OH radicals produced. P25 under UV light produced the highest concentration of OH radicals (16.9 µM), followed by WO₃ (0.56 µM) and Pt-C₃N₄ (0.25 µM). The maximum OH radical production rate for P25, WO₃

and Pt-C₃N₄ were also determined and found to be 35.6 μM/hr, 0.28 μM/hr and 0.88 μM/hr respectively. The other visible light activated photocatalysts did not produce any OH radicals primarily as a result of their electronic structure. Furthermore, it was concluded that, if any visible light absorbing photocatalysts are to be fabricated in future for the purpose of photocatalytic oxidation, their OH radical producing rates (and quantities) should be determined and compared to P25.

Keywords: Photocatalyst, visible light photocatalysts, OH radical, coumarin, P25.

49

50 1. INTRODUCTION

51 Photocatalysis has gained significant interest since the early publication by
 52 Fujishima and Honda in 1972, demonstrating the potential of splitting water over TiO₂
 53 [1]. Since this publication, photocatalysis has been applied to a broad range of fields
 54 including waste water treatment, microbe destruction, toxin removal, energy production
 55 and air treatment. [2-8]. The mechanism of photocatalysis has been well documented
 56 and can be generally represented by the equations shown in reactions 1-9 [9,10]. The
 57 formation of surface radical species such as superoxide (O₂^{•-}) and hydroxyl radicals
 58 (OH[•]) play a key role in a number of photocatalytic pathways and as such their
 59 identification and quantification is a key consideration. As shown in reaction 2, OH
 60 radicals are primarily generated from the reaction between valence band holes (h_{vb}⁺)
 61 and hydroxyl ions on the catalyst surface. An indirect pathway, via O₂^{•-}, also results in
 62 OH radical formation, as shown in reactions 3-6. The efficiency of OH radicals in
 63 photocatalytic reactions is predominantly based on their strong oxidising potential of
 64 2.8 V (vs NHE) [11]. The non-selective nature of these reactive oxygen species also
 65 aids rapid degradation of various pollutants and organic contaminants [3,7,11-16].

66





76 where, h_{vb}^+ represents VB holes and e_{cb}^- means CB electrons.

77

78 Newly developed photocatalytic technologies and materials have often utilised
 79 model compounds and screening methods to assess their performance [17-20].
 80 Common evaluation methods reported in the literature include the decomposition of
 81 dyes such as methylene blue (ISO test 10678:2010), or degradation of organic
 82 pollutants such as 4-chlorophenol or toluene [17-20]. These procedures are often
 83 coupled with the corresponding calculated photonic efficiencies and quantum yields to
 84 evaluate overall efficiency. While these methods can be effective in identifying the
 85 specific photocatalytic performance of a material in relation to a fingerprint compound,
 86 they provide little information regarding the production of OH radicals involved within
 87 the mechanism. Therefore, the requirement for a simple and robust method of radical
 88 quantification for screening the oxidative potential of catalysts has significantly
 89 increased. The challenge in OH radical quantification lies in both the non-selective
 90 nature and short lifetime (~ 1 nanosecond) of the radical, which restricts the possibility
 91 of direct quantification [21]. Consequently, a range of methods have been developed
 92 such as emission spectroscopy, laser induced fluorescence, electron spin resonance,
 93 spin trap and chemical probes or quencher based methods to quantify OH radicals [21-
 94 37].

95

96 The use of a chemical probe to capture OH radicals presents a potentially efficient
 97 way to measure the radical due to the low cost, rapid analysis time and reproducibility
 98 of the method. Monitoring a probe compound through spectroscopy allows the
 99 concentration of OH radicals to be calculated based on stoichiometric ratios of products
 100 formed. A recently reported *in vivo* technique utilised a nanoprobe comprising of a
 101 nanoparticle and azo dye in order to quantify OH radicals in the femtomolar range [37].

Here the nanoparticle was used as an energy donor and the modified orange was used as an OH radical capturing ligand molecule (and the energy acceptor).

Dimethyl sulfoxide (DMSO) based methods for OH radical capture have also been utilised in the past to quantify these species via the formation of formaldehyde [28,29,31]. The formation of CH₄ in a closed system coupled with O₂ bubbling however reduces the suitability of utilising DMSO as a probe molecule.

In the past, OH radical quantification has been carried out for various commercially available photocatalysts, photo-Fenton's reaction and other modified TiO₂ based visible light photocatalysts with either coumarin or terephthalic acid as probe molecules [21,23,31-36,38,39]. Both compounds are capable of acting as OH radical traps by forming fluorescent products as result of reacting with the radical species. Terephthalic acid has been investigated in a study by Ishibashi *et al.* which achieved an OH radical concentration of 7×10^{-5} M based on the measurement of 2-hydroxyterephthalic acid [35]. In addition to the use of terephthalic acid as a probe molecule, coumarin has been used in a number of studies to determine the concentration of OH radicals produced from TiO₂ at relatively high loadings of 1 to 5 g/L [21,23,40]. For instance, Czili *et al.* used 100 µM coumarin as the probe molecule to capture OH radicals under a 40 W UV lamp. They determined a maximum OH radical production rate of 23.39 µM/g/hr (calculated from their reported 7-hydroxycoumarin rates) with 1 g/L TiO₂ P25 photocatalyst.

This paper utilises coumarin as a hydroxyl radical trap and reports the screening of a selection of visible light responsive photocatalysts under low power illumination based on their OH radical producing capability. In contrast to previous reports, which concentrated on quantifying the OH radicals produced from TiO₂, other commercially

available and a few synthesised photocatalysts [21,23,31,40], this work focusses on assessing the oxidative strength of visible light photocatalysts Pt-C₃N₄, 5% LaCr doped SrTiO₃, Sr_{0.95}Cr_{0.05}TiO₃ (referred to as Cr-SrTiO₃ from here on) and yellow TiO₂ and compares them against commercial TiO₂ P25 and WO₃ for evaluation. In addition, a low catalyst loading was used to highlight efficient OH radical formation can be achieved without requiring large quantities of powdered catalyst.

2. EXPERIMENTAL PROCEDURE

2.1 Materials

Coumarin and 7-hydroxycoumarin were purchased from Tokyo Chemical Industry UK Ltd, while TiO₂ P25 was purchased from Degussa (now Evonik industries) and WO₃ nano powders were purchased from Sigma Aldrich. All commercial chemicals were used as received. The catalysts Pt-C₃N₄ [41], 5% LaCr doped SrTiO₃, Cr-SrTiO₃ and yellow TiO₂ [42] were synthesised at the school of chemistry, University of St. Andrews, using methods cited in the literature [41-43].

2.2 Characterisation of Photocatalysts

WO₃, LaCr-SrTiO₃ and Cr-SrTiO₃ were characterised by X-Ray diffraction (XRD) and UV-Visible absorption. XRD analysis of powders was examined on a SToe STADI/P powder diffractometer. Incident radiation was generated using a Cu k_α source (λ=1.54056 Å). Diffuse reflectance spectra were collected on a JASCO-V550 UV-visible spectrophotometer. The characterisation of Pt-C₃N₄ and yellow TiO₂ has been reported elsewhere in literature [41,42].

2.3 Photocatalytic experiments

All photocatalytic experiments were performed in closed screw cap bottles. The reaction solution was composed of 100 ml of 100 μM coumarin along with 10 mg of

photocatalyst (0.1 g/L). A magnetic stirrer bar was placed inside the bottle and the bottle was then placed on a magnetic stirrer at a distance of 11 cm from a 36 W compact fluorescent non-integrated visible lamp (Philips, colour code 830) or a 36 W UV lamp (Philips, Cleo lamps). The spectral outputs of the lamps were measured by a StellaNet spectrometer and the spectra are shown in the supplementary material (Figure S1). Prior to illumination, the reaction solution was stirred in the dark to allow a state of equilibrium to be reached. The length of time required in the dark was calculated from the control experiments conducted in the absence of light. During irradiation, samples (3 mL) were taken at dedicated time intervals for a maximum of 120 mins. Samples were filtered through a 0.22 μm Millex syringe filter prior to analysis. Coumarin absorbance was monitored using a Cary 300 Scan, UV-Visible Spectrophotometer at 277 nm, with a scan rate of 400 nm/min. 7-hydroxycoumarin fluorescence was measured in a PerkinElmer LS 50B luminescence spectrophotometer, using an excitation wavelength of 332 nm and emission wavelength at 456 nm [21]. The excitation and emission slit width was 4 mm and the scan rate was 200 nm/min. A sample UV/Visible and fluorimeter spectra, with peaks at 277 nm and 456 nm respectively, are shown in the supplementary material Figure S2 and Figure S3. All experiments were performed in triplicate.

2.4 OH radical quantification

OH radicals were quantified based on a modified method described by Zhang *et al.* [38] and according to equation 1. The concentration of OH radicals was calculated by assuming that 6.1 % of total OH radicals were captured as 7-hydroxycoumarin. The stoichiometric ratio of one mole of OH radical consumed for the production of one mole of 7-hydroxycoumarin was used [23]. The total number of OH radicals produced over time during this photocatalytic process was calculated using the following equation.

$$X = \left\{ \frac{A}{6.1\%} - B \right\} \dots\dots\dots \text{Equation 1}$$

Where, X is the total OH radical concentration (μM) produced during photocatalysis, A is the mean 7-hydroxycoumarin concentration (μM) and B is the amount of OH radicals (μM) produced during the light control experiments. The concentration of coumarin and 7-hydroxycoumarin was calculated using a standard curve of known concentrations as shown in the supplementary material (Figure S4, Figure S5 and Figure S6).

3. RESULTS AND DISCUSSION

3.1 Characterisation of Photocatalysts

XRD patterns of WO₃, Cr-SrTiO₃ and LaCr-SrTiO₃ samples were determined as shown (Figure 1). The commercial WO₃ nanoparticles exhibited a typical crystallized monoclinic phase structure, and the Cr-doped and La,Cr-co-doped SrTiO₃ samples possessed homogeneous crystallized cubic perovskite structures, with no impurity phase found for either of the doped samples and these results were consistent with literature [44,45]. In the co-doped samples, since La and Cr substitute the Sr and Ti, respectively, and the radius of La is similar with that of Sr while the radius of Cr was similar to that of Ti, the peak positions of the Cr-SrTiO₃ and LaCr-SrTiO₃ samples are not shifted compared to those of pure SrTiO₃.

Figure 1.

In the UV-visible absorption spectra of WO₃, Cr-SrTiO₃ and LaCr-SrTiO₃ (Figure 2), WO₃ exhibited visible light absorption up to 470 nm, which corresponds to the band-gap energy of ca. 2.64 eV. SrTiO₃, however, has no absorption in the visible light region (bandgap of 3.75 eV) and metal-doping has been shown to be a feasible method for extending the light absorption of SrTiO₃ into the visible region [46]. Doping

of Cr into the A-site of SrTiO₃ induces an absorption band in the visible region centred at around 450 nm (Figure 2). The visible light absorption is ascribed to the electron excitation from the Cr doping levels formed above the valence band of SrTiO₃ to the conduction band of SrTiO₃ [43]. It was reported that La, Cr- co-doped SrTiO₃ showed enhanced photocatalytic performance compared to the single Cr-doped SrTiO₃ due to the inhibition of the formation of Cr⁶⁺ species in the B site [43]. Therefore, a co-doped sample, LaCr-SrTiO₃ was prepared by the same method. The visible light absorption of LaCr-SrTiO₃ was significantly enhanced compared to the Cr-SrTiO₃, with two strong absorption peaks centred at around 450 nm and 650 nm in the visible light region. In the case of co-doping, more intermittent doping levels are formed within the band-gap of SrTiO₃ compared to the single Cr doped SrTiO₃, which results in the visible light absorption.

Figure 2.

3.2 Photocatalytic OH radical production

3.2.1 UV light photocatalysis on P25

P25 has been one of the most extensively investigated and most active commercially available photocatalysts under UV irradiation and therefore was used as a benchmark for comparison in this study. Although, recent studies have reported that nano-spherical InCrO₄-loaded TiO₂ and TiO₂ nanospheres deposited on graphene performed better than P25 for OH radical production and dye degradation upon UV irradiation [47,48], to date P25 is still regarded as the benchmark. The photocatalytic hydroxylation of coumarin over P25 under UV light and subsequent formation of 7-hydroxycoumarin is shown in Figure 3. The production of 7-hydroxycoumarin under these conditions equates to a peak OH radical concentration of 16.9 µM after 45 mins.

Figure 3.

As shown in the figure, near complete degradation (97 %) of coumarin was achieved after 120 mins irradiation. This level of degradation was likely to result from the increased adsorption of coumarin onto the catalyst, which facilitated the reaction with surface bound OH radicals. The role of surface bound radicals and those that are present in bulk has been highlighted in a previous publication by Li *et al.* [49], who investigated acid orange oxidation over TiO₂ P25 and AgBr. This group investigated the quenching of OH radicals at the catalyst surface and in bulk in order to demonstrate that surface bound species were the predominant radicals in the oxidation pathway. This observation confirmed that increased adsorption of the substrate on the catalyst surface can significantly increase the degradation efficiency.

Figure 3 also shows the profile of 7-hydroxycoumarin production and decomposition which indirectly indicates the quantity of OH radicals generated. 7-hydroxycoumarin concentration peaked at 45 minutes, with a maximum concentration of 1.045 μM , which was equivalent to 16.9 μM OH radicals (as calculated from equation 1). It was observed that an average production rate of 1.8 $\mu\text{M/hr}$ was achieved during the first 45 mins, followed by an average degradation rate of 0.46 $\mu\text{M/hr}$ during the latter stages of irradiation. The decrease in concentration of 7-hydroxycoumarin could also be attributed to the presence of superoxide radicals as reported by Czili and Horvath [23].

Several reports have suggested the kinetics for 7-hydroxycoumarin generation from coumarin with P25 under UV irradiation are zero order [21,23,38,50-52], however, a number of these investigations also used a high concentration of both catalyst and coumarin. Furthermore, it has been suggested that at higher concentrations of coumarin (>100 μM), more UV light is absorbed by this probe and not the catalyst,

which results in a low 7-hydroxycoumarin and OH radical production rate [23]. In the present study, K_{app} which is the rate constant for the formation of 7-hydroxycoumarin was calculated to be 0.0234 $\mu\text{M}/\text{min}$ whereas K_{dis} , the rate constant for the disappearance of 7-hydroxycoumarin was calculated to be 0.0135 $\mu\text{M}/\text{min}$. In this study we have established that both, production and degradation of 7-hydroxycoumarin followed zero order kinetics, which is agreement with previous studies.

3.2.2 Visible light photocatalysis

A number of visible light catalysts were also selected for comparison against P25 TiO_2 . While the synthesised catalysts all possessed energy band gaps that supported visible light activation, only WO_3 and $\text{Pt-C}_3\text{N}_4$ had energy band potentials (valence band at 3.2 V and 1.4 V respectively and conduction band at 0.2 V and -1.3 V respectively) that would facilitate OH radical formation either directly or indirectly as mentioned in reactions 2–6. Catalysts LaCr-SrTiO_3 , Cr-SrTiO_3 and yellow TiO_2 (valence bands at 2.7 V, 2.7 V and 2.6 V respectively and conduction bands at -0.1 V for all the three photocatalysts) were selected to monitor if 7-hydroxycoumarin was formed even when the electronic structure of the catalyst was not suited to the redox potential of the reaction.

The photocatalytic hydroxylation of coumarin to 7-hydroxycoumarin over WO_3 and $\text{Pt-C}_3\text{N}_4$ under visible light is shown in Figure 4. As can be seen, minimal conversion of coumarin was observed over both $\text{Pt-C}_3\text{N}_4$ and WO_3 , which was also supported by the low formation of 7-hydroxycoumarin (Figure 5). $\text{Pt-C}_3\text{N}_4$ displayed a slow yet steady conversion rate, reaching a 0.91 % drop in coumarin after 120 mins of irradiation whereas, a varying coumarin concentration pattern was seen over time on WO_3 . It is interesting to note that there was an initial decrease in coumarin concentration followed by an increase which may be attributed to coumarin desorption from the surface of

WO₃. This desorption could be a result of the alteration in equilibrium in the closed system due to the possible evolution of O₂ from water on WO₃ under visible light.

Figure 4.

While the decrease in coumarin concentration is low, production of OH radicals over Pt-C₃N₄ and WO₃ was supported by the detection of 7-hydroxycoumarin upon photocatalysis (Figure 5). When WO₃ was used as the photocatalyst, there was no 7-hydroxycoumarin production until 30 minutes of irradiation which could be due to the rapid recombination of the electrons and the photo generated holes. After 30 minutes, OH radical production was steady with a gradual generation of 7-hydroxycoumarin being observed. In the case of Pt-C₃N₄ however, 7-hydroxycoumarin production was seen from 15 minutes. The initial increase in the 7-hydroxycoumarin concentration correlates to a rapid degradation of coumarin during the first 60 mins of irradiation.

Figure 5.

In contrast to Pt-C₃N₄ and WO₃, the catalysts LaCr-SrTiO₃, Cr-SrTiO₃ and yellow TiO₂ displayed no activity towards coumarin conversion to 7-hydroxycoumarin, which indicates no OH radical formation. Furthermore, under prolonged visible light irradiation no detectable 7-hydroxycoumarin was recorded.

3.2.3 Influence of photocatalysts' electronic structure and particle size on OH radical formation

In order to evaluate and discuss the performance of the catalysts, it is essential to consider the primary contributing factors; electronic structure and particle size. The electronic structure of the catalysts dictates the initial photo-excitation of electrons to

higher energy levels, while the particle size dictates the concentration of photons absorbed and surface reactions between coumarin and OH radicals. As shown in reactions (2) – (6), OH radicals can occur via two routes in photocatalysis. The direct formation at the valence band requires a redox potential of 2.8 V vs NHE, while the indirect method occurs via the intermediate radical, $O_2^{\cdot-}$ and requires a redox potential of -0.33 V vs NHE [53]. The electronic structure of the catalysts tested in this study, in relation to the redox potentials required for radical formation, are shown in Figure 6.

Figure 6

As Figure 6 shows, catalysts TiO_2 P25, $Pt-C_3N_4$ and WO_3 possess an electronic structure which corresponds to the redox potential of OH radical formation via either direct or indirect mechanisms. The favourable electronic structure of TiO_2 for OH radical formation has been well documented and is evident from the results highlighted here. The performance of $Pt-C_3N_4$ and WO_3 for OH radical formation, however, has not been as well reported. The structure of WO_3 with a more positive valence band suggests it is capable of generating surface OH radicals, however, the results obtained indicate minimal 7-hydroxycoumarin production within 2 hours. Based on the structure, it was likely an increased rate of recombination preventing OH radical formation via the valence band hole, due to insufficient energy to initiate a reduction reaction at the conduction band [21]. To prevent recombination and to increase the OH radical production, Kim *et al.* synthesised Pt-doped WO_3 and found that the OH radical production from Pt- WO_3 was significantly higher than un-doped WO_3 [20]. Furthermore, the large particle size of approximately 100 nm for WO_3 indicates a smaller surface area, which leads to minimum absorption of light.

The electronic structure of Pt-C₃N₄ as seen from Figure 6 clearly indicates a reducing catalyst, which is also supported by its application in water reduction investigations [54]. Therefore, the hydroxylation of coumarin and subsequent formation of 7-hydroxycoumarin, as indicated by the earlier results, is likely via the indirect O₂^{•-} pathway. Based upon this observation, it is likely the low yield of OH radicals is a result of competition for the conduction band electron between superoxide formation and H⁺ reduction to form H₂ (0 V vs NHE). In addition, since all these experiments were performed in a closed system with limited O₂, a reducing catalyst such as Pt-C₃N₄ is expected to produce less OH radicals than an open system. Furthermore, despite a favourable particle size of 20-40 nm, Pt-C₃N₄ was observed to agglomerate to form larger aggregates leading to a decrease in surface area and in turn light absorption.

In the case of LaCr-SrTiO₃, Cr-SrTiO₃ and yellow TiO₂, the electronic structures showed both the valence band and conduction band of all these catalysts to be lower than the redox potentials to facilitate radical formation as seen in Figure 6. These catalysts were primarily used as a control parameter to ensure no 7-hydroxycoumarin formation was observed.

The calculated OH radical concentrations and production rates produced over all catalysts screened are summarised in Table 1. The results show that the activity of the visible light activated photocatalysts studied were significantly lower than commercial P25 under UV light. This further emphasises that although there are numerous visible light absorbing photocatalysts, their ability to produce OH radicals is significantly lower than P25. In future, if any visible light absorbing photocatalysts are to be fabricated for the purpose of photocatalytic oxidation, their OH radical producing rates (and quantities) should be determined and compared to P25 as demonstrated here.

Table 1

4. CONCLUSION

The aim of screening UV and visible light absorbing photocatalysts to assess their oxidative strength was accomplished successfully by trapping OH radicals produced by the photocatalysts in 7-hydroxycoumarin. The OH radical production capabilities of various photocatalysts covering a range of band gaps and particle sizes were assessed by comparing and discussing their differences with the commercial UV light activated P25. To conclude, visible light activated photocatalysts such as LaCr-SrTiO₃, Cr-SrTiO₃ and yellow TiO₂ did not produce any OH radicals and this could be attributed to their electronic structure. Whereas, the (pseudo) maximum OH radical production rates of other visible light activated photocatalysts namely, WO₃ (0.28 µM/hr) and Pt-C₃N₄ (0.886 µM/hr) were found to be significantly lower when compared to the commercial UV light activated P25 photocatalyst (35.654 µM/hr). This method could be further exploited as novel photocatalysts are developed and to compare a range of P25 concentrations for OH radical production. This study further emphasises the challenges faced by the visible light photocatalysts for photocatalytic oxidation.

5. ACKNOWLEDGEMENTS

This work was supported by the Engineering and Physical Sciences Research Council (Project number EP/K036769/1), Robert Gordon University's IDEAS PhD studentship and Queen's University Belfast's PhD studentship. The author would also like to thank Professor A Prasanna de Silva, School of Chemistry and Chemical Engineering, Queen's University Belfast, for his valuable contribution during the progress meetings. Supporting data are openly available on Queen's University, Belfast Research Portal, [http:// pure.qub.ac.uk/portal/en/datasets/search.html](http://pure.qub.ac.uk/portal/en/datasets/search.html).

REFERENCES

- [1] A. Fujishima, K. Honda, Electrochemical Photolysis of Water at a Semiconductor Electrode, *Nature*. 238 (1972) 37-38.
- [2] D.W. Bahnemann, L.A. Lawton, P.K.J. Robertson, The Application of Semiconductor Photocatalysis for the Removal of Cyanotoxins from Water and Design Concepts for Solar Photocatalytic Reactors for Large Scale Water Treatment, in: S.L. Suib (Ed.), *New and Future Developments in Catalysis*, 1st ed., Elsevier, Amsterdam, 2013, pp. 395-415.
- [3] M.R. Hoffmann, S.T. Martin, W. Choi, D.W. Bahnemann, Environmental Applications of Semiconductor Photocatalysis, *Chem. Rev.* 95 (1995) 69-96.
- [4] P.K.J. Robertson, J.M.C. Robertson, D.W. Bahnemann, Removal of microorganisms and their chemical metabolites from water using semiconductor photocatalysis, *J. Hazard. Mater.* 211–212 (2012) 161-171.
- [5] H. Kominami, S. Murakami, M. Kohno, Y. Kera, K. Okada, B. Ohtani, Stoichiometric decomposition of water by titanium(IV) oxide photocatalyst synthesized in organic media: Effect of synthesis and irradiation conditions on photocatalytic activity, *Phys. Chem. Chem. Phys.* 3 (2001) 4102-4106.
- [6] C. McCullagh, P.K.J. Robertson, M. Adams, P.M. Pollard, A. Mohammed, Development of a slurry continuous flow reactor for photocatalytic treatment of industrial waste water, *J. Photochem. Photobiol. A*. 211 (2010) 42-46.
- [7] P.K.J. Robertson, Semiconductor photocatalysis: an environmentally acceptable alternative production technique and effluent treatment process, *J. Clean. Prod.* 4 (1996) 203-212.
- [8] M. Adams, I. Campbell, C. McCullagh, D. Russell, D.W. Bahnemann, P.K.J. Robertson, From Ideal Reactor Concepts to Reality: The Novel Drum Reactor for Photocatalytic Wastewater Treatment, *Int. J. Chem. React. Eng.* 11 (2013) 621-632.
- [9] O. Carp, C.L. Huisman, A. Reller, Photoinduced reactivity of titanium dioxide, *Progress in Solid State Chemistry*. 32 (2004) 33-177.
- [10] C. McCullagh, N. Skillen, M. Adams, P.K.J. Robertson, Photocatalytic reactors for environmental remediation: a review, *J. Chem. Technol. Biotechnol.* 86 (2011) 1002-1017.
- [11] J. Jiang, Z. Zhou, V.K. Sharma, Occurrence, transportation, monitoring and treatment of emerging micro-pollutants in waste water — A review from global views, *Microchem. J.* 110 (2013) 292-300.
- [12] A. Asghar, A.A. Abdul Raman, W.M.A. Wan Daud, Advanced oxidation processes for in-situ production of hydrogen peroxide/hydroxyl radical for textile wastewater treatment: a review, *J. Clean. Prod.* 87 (2015) 826-838.

- 435 [13] H. Fan, G. Li, F. Yang, L. Yang, S. Zhang, Photodegradation of cellulose under UV
436 light catalysed by TiO₂, *J. Chem. Technol. Biotechnol.* 86 (2011) 1107-1112.
- 437 [14] E. Szabó-Bárdos, K. Somogyi, N. Törő, G. Kiss, A. Horváth, Photocatalytic
438 decomposition of L-phenylalanine over TiO₂: Identification of intermediates and the
439 mechanism of photodegradation, *Appl. Catal. B: Environ.* 101 (2011) 471-478.
- 440 [15] T. Hirakawa, K. Yawata, Y. Nosaka, Photocatalytic reactivity for O₂⁻ and OH
441 radical formation in anatase and rutile TiO₂ suspension as the effect of H₂O₂ addition,
442 *Appl. Catal. A-Gen.* 325 (2007) 105-111.
- 443 [16] Y. Nosaka, T. Daimon, A.Y. Nosaka, Y. Murakami, Singlet oxygen formation in
444 photocatalytic TiO₂ aqueous suspension, *Phys. Chem. Chem. Phys.* 6 (2004) 2917-
445 2918.
- 446 [17] X. Yan, T. Ohno, K. Nishijima, R. Abe, B. Ohtani, Is methylene blue an appropriate
447 substrate for a photocatalytic activity test? A study with visible-light responsive titania,
448 *Chemical Physics Letters*. 429 (2006) 606-610.
- 449 [18] B. Ohtani, Preparing Articles on Photocatalysis—Beyond the Illusions,
450 Misconceptions, and Speculation, *Chem. Lett.* 37 (2008) 216-229.
- 451 [19] A. Mills, An overview of the methylene blue ISO test for assessing the activities of
452 photocatalytic films, *Applied Catalysis B: Environmental*. 128 (2012) 144-149.
- 453 [20] J. Kim, C.W. Lee, W. Choi, Platinized WO₃ as an Environmental Photocatalyst that
454 Generates OH Radicals under Visible Light, *Environ. Sci. Technol.* 44 (2010) 6849-
455 6854.
- 456 [21] Q. Xiang, J. Yu, P.K. Wong, Quantitative characterization of hydroxyl radicals
457 produced by various photocatalysts, *J. Colloid Interface Sci.* 357 (2011) 163-167.
- 458 [22] M. Sato, T. Ohgizama, J.S. Clements, Formation of chemical species and their
459 effects on microorganisms using a pulsed high voltage discharge in water, *Industry*
460 *Applications Society Annual Meeting*. 2 (1994) 1455-1461.
- 461 [23] H. Czili, A. Horváth, Applicability of coumarin for detecting and measuring hydroxyl
462 radicals generated by photoexcitation of TiO₂ nanoparticles, *Appl. Catal. B: Environ.* 81
463 (2008) 295-302.
- 464 [24] R. Ono, T. Oda, Measurement of hydroxyl radicals in pulsed corona discharge, *J.*
465 *Electrostatics*. 55 (2002) 333-342.
- 466 [25] W. Hoeben, E. van Veldhuizen, W. Rutgers, G. Kroesen, Gas phase corona
467 discharges for oxidation of phenol in an aqueous solution, *J. Phys. D: Appl. Phys.* 32
468 (1999) 133-137.
- 469 [26] P. Sunka, V. Babický, M. Clupek, P. Lukes, M. Simek, J. Schmidt, M. Cern,
470 Generation of chemically active species by electrical discharges in water, *Plasma*
471 *Sources Sci. Technol.* 8 (1999) 258-265.

472 [27] B. Sun, M. Sato, J. Sid Clements, Optical study of active species produced by a
473 pulsed streamer corona discharge in water, *J. Electrostatics*. 39 (1997) 189-202.

474 [28] M.G. Steiner, C.F. Babbs, Quantitation of the hydroxyl radical by reaction with
475 dimethyl sulfoxide, *Arch. Biochem. Biophys.* 278 (1990) 478-481.

476 [29] M. Sahni, B.R. Locke, Quantification of Hydroxyl Radicals Produced in Aqueous
477 Phase Pulsed Electrical Discharge Reactors, *Ind. Eng. Chem. Res.* 45 (2006) 5819-
478 5825.

479 [30] J. Ku, E. Zimowski, United States Department of Labor, Occupational Safety and
480 Health Administration. 3M Formaldehyde Monitor (Model 3721), Product evaluation
481 (PE-10). 205 (1989).

482 [31] S.A.V. Eremia, D. Chevalier-Lucia, G. Radu, J. Marty, Optimization of hydroxyl
483 radical formation using TiO₂ as photocatalyst by response surface methodology,
484 *Talanta*. 77 (2008) 858-862.

485 [32] T. Maezono, M. Tokumura, M. Sekine, Y. Kawase, Hydroxyl radical concentration
486 profile in photo-Fenton oxidation process: Generation and consumption of hydroxyl
487 radicals during the discoloration of azo-dye Orange II, *Chemosphere*. 82 (2011) 1422-
488 1430.

489 [33] M. Tokumura, R. Morito, R. Hatayama, Y. Kawase, Iron redox cycling in hydroxyl
490 radical generation during the photo-Fenton oxidative degradation: Dynamic change of
491 hydroxyl radical concentration, *Appl. Catal. B: Environ.* 106 (2011) 565-576.

492 [34] S. Kanazawa, T. Furuki, T. Nakaji, S. Akamine, R. Ichiki, Measurement of OH
493 Radicals in Aqueous Solution Produced by Atmospheric-pressure LF Plasma Jet, *I. J.*
494 *PEST*. 6 (2012) 166-171.

495 [35] K. Ishibashi, A. Fujishima, T. Watanabe, K. Hashimoto, Quantum yields of active
496 oxidative species formed on TiO₂ photocatalyst, *J. Photochem. Photobiol. A*. 134
497 (2000) 139-142.

498 [36] T. Hirakawa, Y. Nosaka, Properties of O₂⁻ and OH[•] Formed in TiO₂ Aqueous
499 Suspensions by Photocatalytic Reaction and the Influence of H₂O₂ and Some Ions,
500 *Langmuir*. 18 (2002) 3247-3254.

501 [37] Z. Li, T. Liang, S. Lv, Q. Zhuang, Z. Liu, A Rationally Designed Upconversion
502 Nanoprobe for in Vivo Detection of Hydroxyl Radical, *J. Am. Chem. Soc.* 137 (2015)
503 11179-11185.

504 [38] J. Zhang, Y. Nosaka, Quantitative Detection of OH Radicals for Investigating the
505 Reaction Mechanism of Various Visible-Light TiO₂ Photocatalysts in Aqueous
506 Suspension, *J. Phys. Chem. C*. 117 (2013) 1383-1391.

507 [39] M.E. Lindsey, M.A. Tarr, Quantitation of hydroxyl radical during Fenton oxidation
508 following a single addition of iron and peroxide, *Chemosphere*. 41 (2000) 409-417.

509 [40] J. Zhang, Y. Nosaka, Generation of OH radicals and oxidation mechanism in
510 photocatalysis of WO₃ and BiVO₄ powders, *J. Photochem. Photobiol. A.* 303–304
511 (2015) 53-58.

512 [41] F. Fina, H. Menard, J.T.S. Irvine, The effect of Pt NPs crystallinity and distribution
513 on the photocatalytic activity of Pt-g-C₃N₄, *Phys. Chem. Chem. Phys.* 17 (2015)
514 13929-13936.

515 [42] C. Randorn, J.T.S. Irvine, P. Robertson, Synthesis of Visible-Light-Activated
516 Yellow Amorphous Photocatalyst, *Int. J. Photoenergy.* 2008 (2008) 1-6.

517 [43] S. Ouyang, H. Tong, N. Umezawa, J. Cao, P. Li, Y. Bi, Y. Zhang, J. Ye, Surface-
518 Alkalinization-Induced Enhancement of Photocatalytic H₂ Evolution over SrTiO₃-Based
519 Photocatalysts, *J. Am. Chem. Soc.* 134 (2012) 1974-1977.

520 [44] M. Muralidharan, V. Anbarasu, A. Elaya Perumal, K. Sivakumar, Carrier mediated
521 ferromagnetism in Cr doped SrTiO₃ compounds, *J. Mater. Sci. : Mater. Electron.* 26
522 (2015) 6352-6365.

523 [45] J. Guo, Y. Li, S. Zhu, Z. Chen, Q. Liu, D. Zhang, W. Moon, D. Song, Synthesis of
524 WO₃@Graphene composite for enhanced photocatalytic oxygen evolution from water,
525 *RSC Adv.* 2 (2012) 1356-1363.

526 [46] K. van Benthem, C. Elsässer, R.H. French, Bulk electronic structure of SrTiO₃:
527 Experiment and theory, *J. Appl. Phys.* 90 (2001) 6156-6164.

528 [47] J. Kamalakkannan, V.L. Chandraboss, S. Prabha, S. Senthilvelan, Advanced
529 construction of heterostructured InCrO₄-TiO₂ and its dual properties of greater UV-
530 photocatalytic and antibacterial activity, *RSC Adv.* 5 (2015) 77000-77013.

531 [48] M. Wojtoniszak, B. Zielinska, R.J. Kalenczuk, E. Mijowska, Photocatalytic
532 performance of titania nanospheres deposited on graphene in coumarin oxidation
533 reaction, *Materials Science-Poland.* 30 (2012) 32-38.

534 [49] G. Li, K.H. Wong, X. Zhang, C. Hu, J.C. Yu, R.C.Y. Chan, P.K. Wong, Degradation
535 of Acid Orange 7 using magnetic AgBr under visible light: The roles of oxidizing
536 species, *Chemosphere.* 76 (2009) 1185-1191.

537 [50] J. Zhang, Y. Nosaka, Mechanism of the OH Radical Generation in Photocatalysis
538 with TiO₂ of Different Crystalline Types, *J. Phys. Chem. C.* 118 (2014) 10824-10832.

539 [51] H. Guan, L. Zhu, H. Zhou, H. Tang, Rapid probing of photocatalytic activity on
540 titania-based self-cleaning materials using 7-hydroxycoumarin fluorescent probe, *Anal.*
541 *Chim. Acta.* 608 (2008) 73-78.

542 [52] Z. Huang, Q. Sun, K. Lv, Z. Zhang, M. Li, B. Li, Effect of contact interface between
543 TiO₂ and g-C₃N₄ on the photoreactivity of g-C₃N₄/TiO₂ photocatalyst: (0 0 1) vs (1 0
544 1) facets of TiO₂, *Applied Catalysis B: Environmental.* 164 (2015) 420-427.

545 [53] P.M. Wood, The potential diagram for oxygen at pH 7, *Biochem. J.* 253 (1988)
546 287-289.

547 [54] G. Zhang, Z. Lan, L. Lin, S. Lin, X. Wang, Overall water splitting by Pt/g-C₃N₄
548 photocatalysts without using sacrificial agents, Chem. Sci. 7 (2016) 3062-3066.

549

550 **List of Captions for figures and tables.**

551 Figure 1: XRD profiles of photocatalysts representing the plane indices [44,45].

552 Figure 2: UV-Visible absorption spectra of photocatalysts

553 Figure 3: Coumarin and 7-hydroxycoumarin profiles of 100 ml of 100 μ M coumarin with
554 0.1 g/L P25 under 36 W UV light

555 Figure 4: Coumarin profiles of 100 ml of 100 μ M coumarin with 0.1 g/L visible light
556 photocatalysts; Inset: coumarin profiles of WO_3 and $\text{Pt-C}_3\text{N}_4$

557 Figure 5: 7-hydroxycoumarin production profiles of 100 ml of 100 μ M coumarin with 0.1
558 g/L visible light photocatalysts

559 Figure 6: Electronic structure of the photocatalysts used

560

561 Table 1: Pseudo maximum OH radical production rates and quantities.

562

563

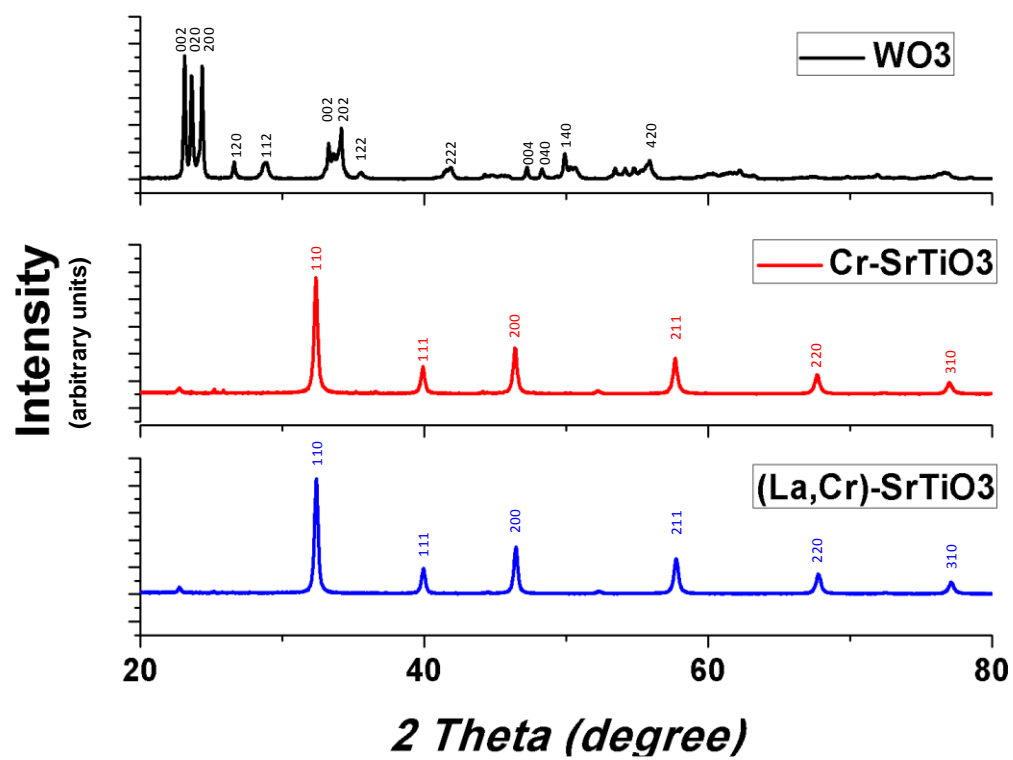


Figure 1

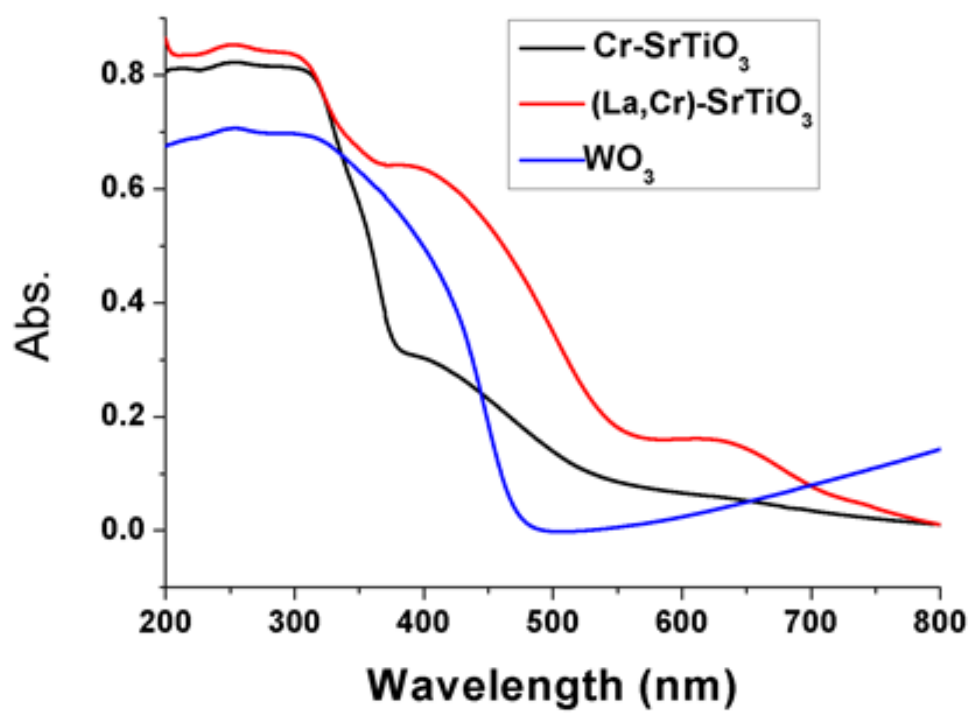


Figure 2

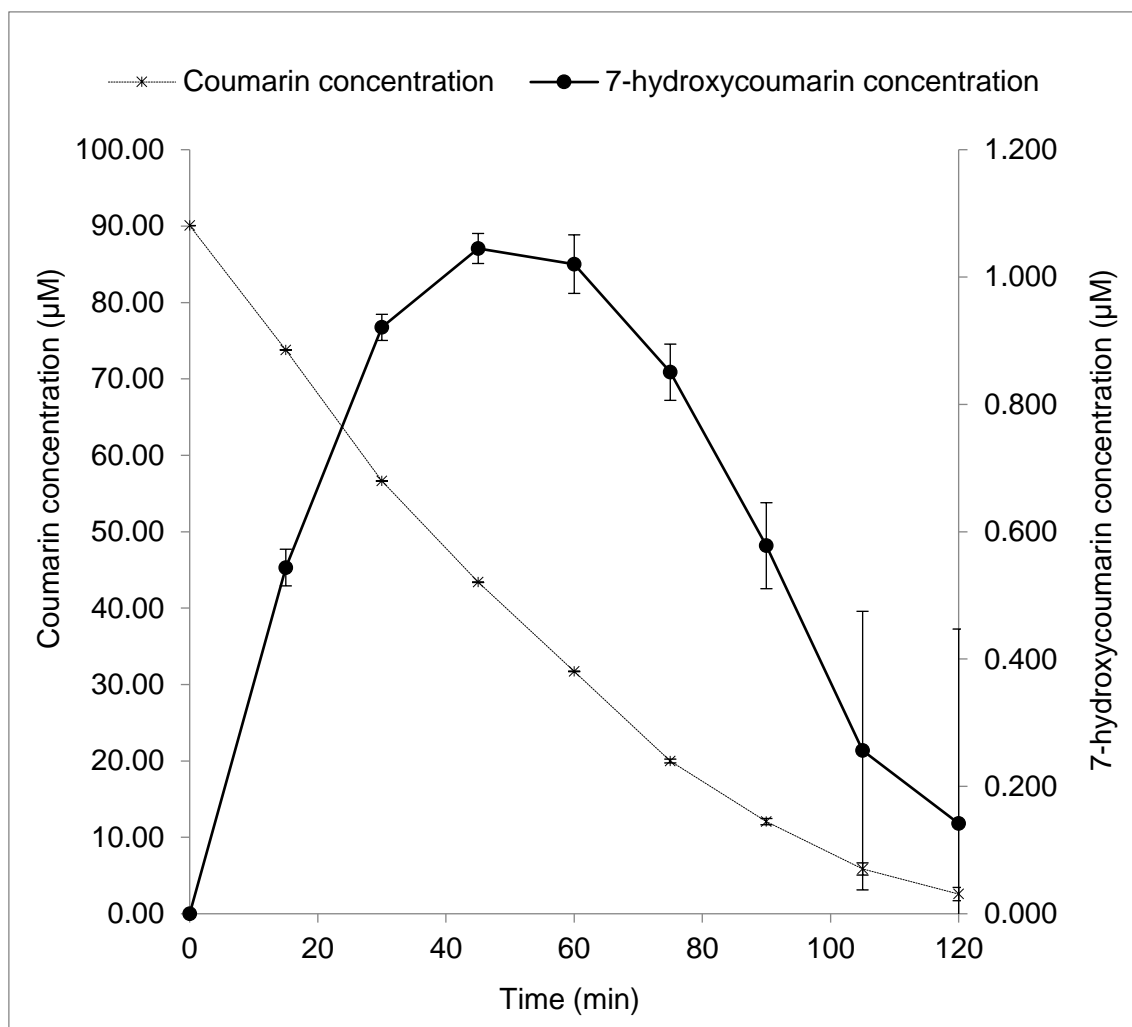
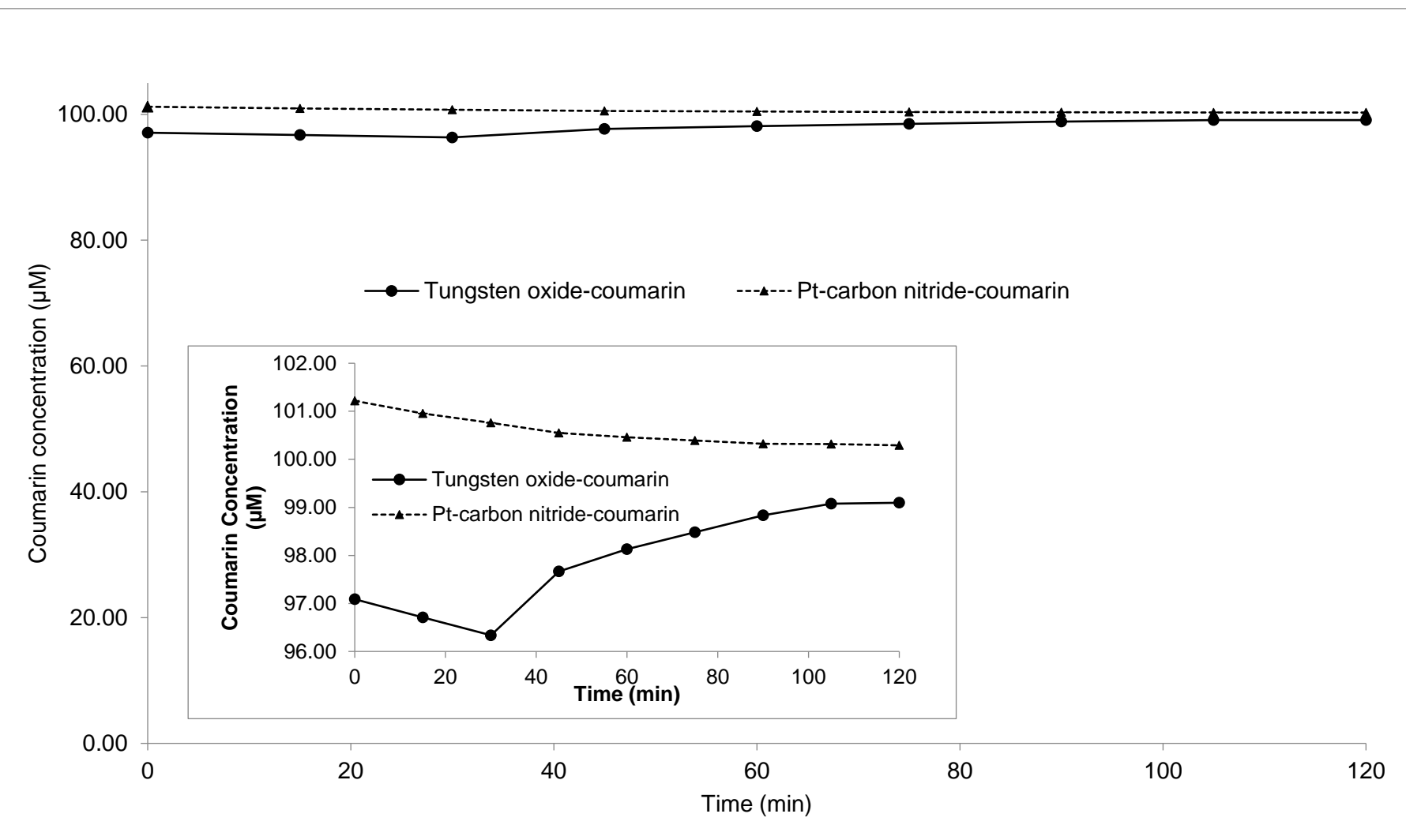


Figure 3



580

581 **Figure 4**

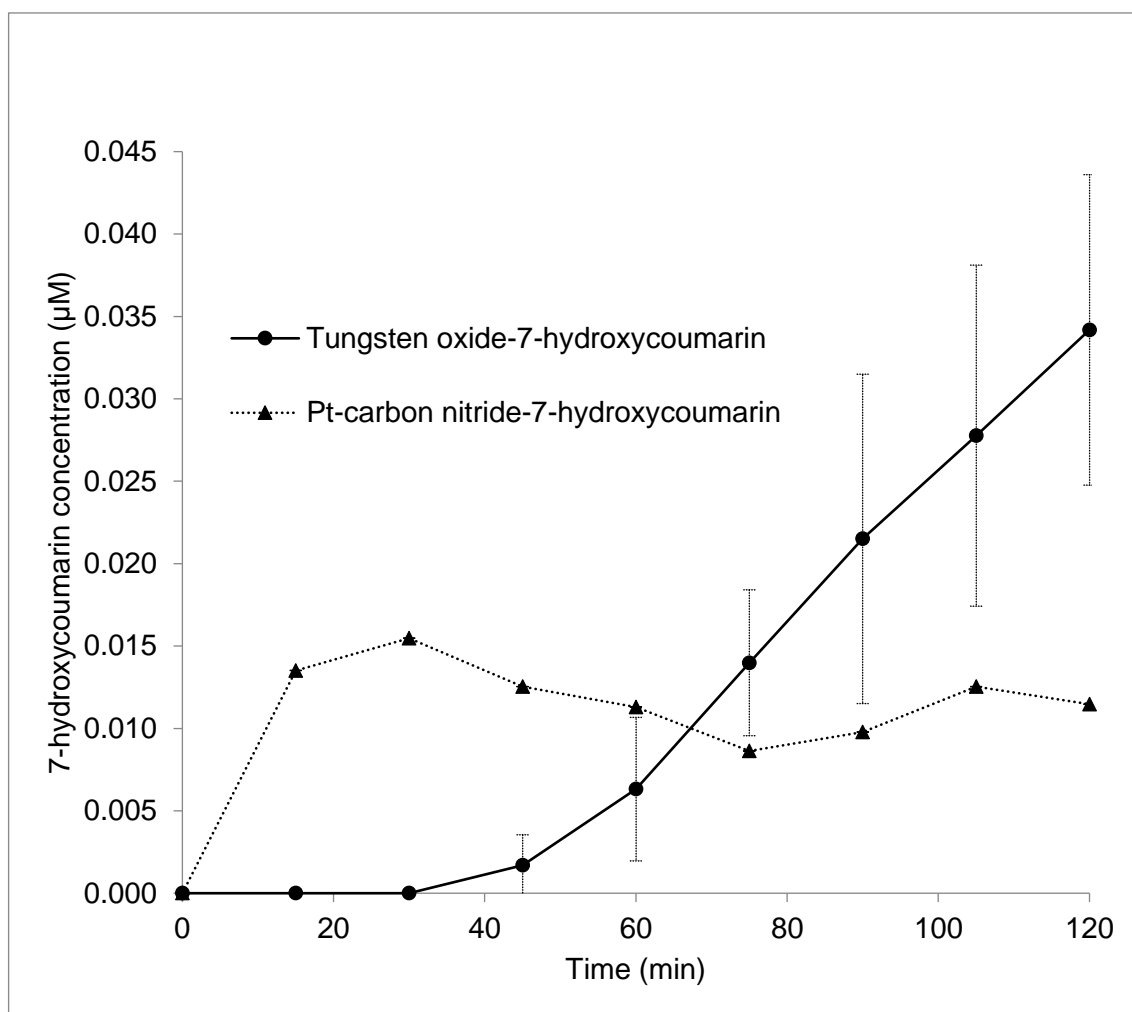


Figure 5

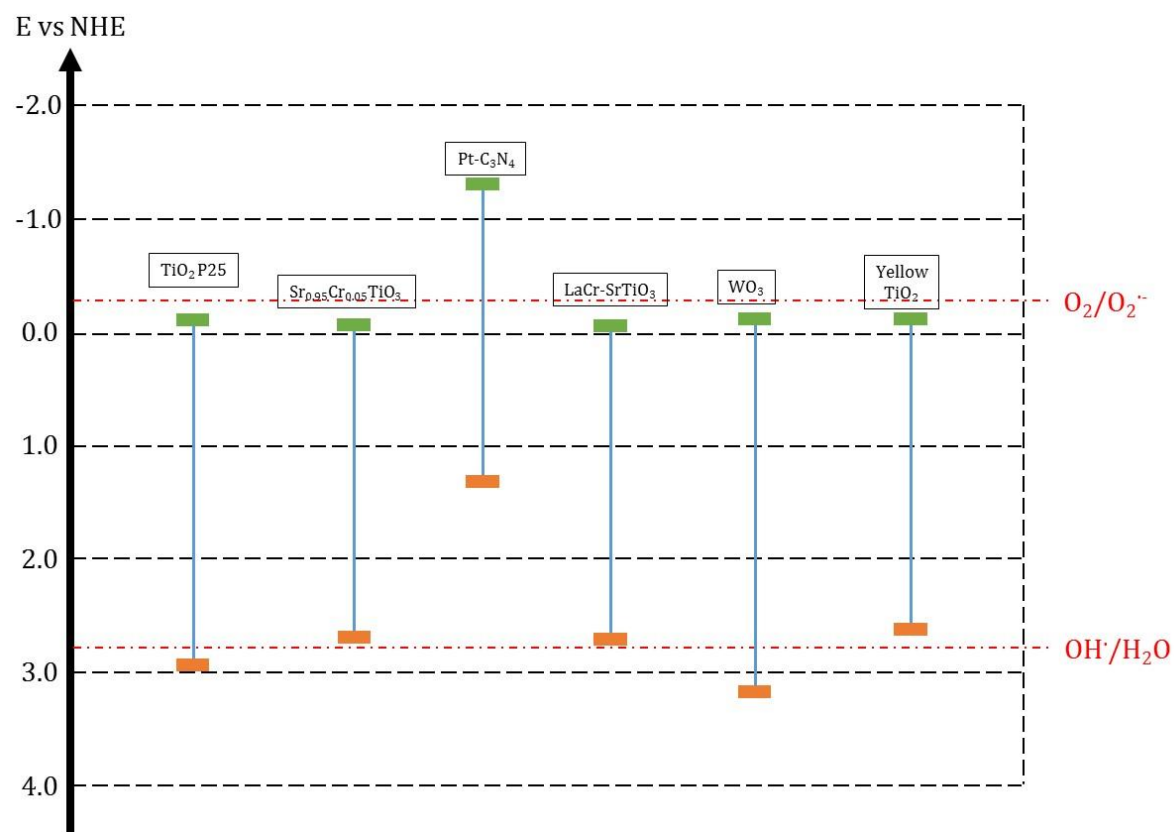


Figure 6

Photocatalyst	Light Source	Maximum OH radical concentration (μM)	Time at which maximum concentration of OH radical was produced (min)	Maximum OH radical production rate ($\mu\text{M/hr}$)
P25	UV	16.9	45	35.654
WO_3	visible	0.560	120	0.280
$\text{Pt-C}_3\text{N}_4$	visible	0.254	30	0.886

609

610 **Table 1**